ARTICLES
https://doi.org/10.1038/s41567-019-0538-0
nature physics

Polaron spin dynamics in high-mobility polymeric semiconductors

Sam Schott[1], Uday Chopra[2,3], Vincent Lemaur[4], Anton Melnyk[5], Yoan Olivier[4], Riccardo Di Pietro[6], Igor Romanov[1], Remington L. Carey[1], Xuechen Jiao[7,8], Cameron Jellett[9], Mark Little[9], Adam Marks[9], Christopher R. McNeill[7], Iain McCulloch[9,10], Erik R. McNellis[2], Denis Andrienko[5], David Beljonne[4], Jairo Sinova[2] and Henning Sirringhaus[1*]

Polymeric semiconductors exhibit exceptionally long spin lifetimes, and recently observed micrometre spin diffusion lengths in conjugated polymers demonstrate the potential for organic spintronics devices. Weak spin–orbit and hyperfine interactions lie at the origin of their long spin lifetimes, but the coupling mechanism of a spin to its environment remains elusive. Here, we present a systematic study of polaron spin lifetimes in field-effect transistors with high-mobility conjugated polymers as an active layer. We demonstrate how spin relaxation is governed by the charges' hopping motion at low temperatures, whereas an Elliott–Yafet-like relaxation due to a transient localization of the carrier wavefunctions is responsible for spin relaxation at high temperatures. In this regime, charge, spin and structural dynamics are intimately related and depend sensitively on the local conformation of polymer backbones and the crystalline packing of the polymer chains.

Spin is a fundamental quantum-mechanical property of electrons in metals and semiconductors that governs many of their physical properties and is being exploited directly in the fields of spintronics and quantum information processing. It is a particularly important quantum number also for organic semiconductors, where spin governs, for example, the fundamental photophysics of singlet and triplet excitons in organic light-emitting and photovoltaic diodes[1–3] or gives rise to large magnetoresistance effects[4,5]. Its importance in these mainly carbon-based materials originates from inefficient pathways for spin relaxation—in particular through weak hyperfine interactions (HFIs) and spin–orbit coupling—that results in long spin lifetimes compared with most inorganic materials. Recent reports of 100–1,000 nm spin diffusion lengths[6,7], spin-to-charge conversion[8,9] or techniques to control the spin polarization at molecule–ferromagnet 'spinterfaces'[10] may even lead to applications of polymeric and molecular semiconductors in spintronic devices.

Given the importance of spin, it may be surprising that the microscopic mechanisms for spin relaxation are not better understood in organic materials. The strengths of HFIs and spin–orbit coupling have recently been investigated at a molecular level, depending on the elemental composition and geometry of the conjugated systems[11–14]. However, the relationship between charge motion and spin dynamics has only been studied for a few model systems[15–19] and remains poorly understood, in particular for state-of-the-art conjugated polymers with high charge-carrier mobilities.

Interactions that result in spin-lattice relaxation and decoherence, with the respective timescales T_1 and T_2, can be treated as effective magnetic fields which fluctuate in the spin's rest frame. In organic materials, they are closely linked to charge transport as charges move through a molecular lattice with different local field environments. Simultaneously, spin relaxation should also be affected by intra- and intermolecular vibrations which modulate the spin–orbit coupling and HFIs. Accordingly, theoretical treatments have distinguished between three spin relaxation mechanisms[20]: motional[21], Elliott–Yafet (EY)[22,23] and intra-site relaxation[24]. Understanding spin relaxation at a microscopic level is not merely worthwhile in itself, but would also lead to a more microscopic understanding of charge dynamics.

Spin transport in solid organic films has been probed most commonly along the low-mobility out-of-plane direction, in organic spin valves[25–28], by spin pumping[6,29], or by electrically and optically detected spin resonance[30,31], but accurately determining polaron spin lifetimes has been challenging. Values inferred from organic spin valves[32] or spin-pumping measurements[6] range between 10 µs and 1,000 µs, and may suffer from device-related artifacts[33–35]. On the other hand, field-induced electron spin resonance (FI-ESR) measurements provide a more direct way to unambiguously identify the spin signature associated with polaronic carriers and have consistently shown shorter spin lifetimes of the order of 10 ns to 10 µs (refs. [16,18,19]). This discrepancy may arise in part from estimating T_1 by relating the charge diffusion constant D to the spin diffusion length λ_S in the kinetic equation $\lambda_S = \sqrt{DT_1}$. Here, D is determined from the charge carrier mobility by the Einstein relation[36,37], and λ_S is extracted from devices with different organic layer thicknesses. Together with the absence of a Hanle effect in many such measurements, the exceedingly large T_1 values have cast doubt on equating charge and spin diffusion constants and raised questions about the nature of spin transport in organic semiconductors[29,38].

Here, we perform FI-ESR measurements on a range of high-mobility conjugated polymers. Our aim is to measure spin

[1]Cavendish Laboratory, University of Cambridge, Cambridge, UK. [2]INSPIRE Group, Johannes Gutenberg University, Mainz, Germany. [3]Graduate School of Excellence Materials Science in Mainz, Mainz, Germany. [4]Laboratory for Chemistry of Novel Materials, University of Mons, Mons, Belgium. [5]Max Planck Institute for Polymer Research, Mainz, Germany. [6]Hitachi Cambridge Laboratory, Cambridge, UK. [7]Department of Materials Science and Engineering, Monash University, Clayton, Victoria, Australia. [8]Australian Synchrotron, ANSTO, Clayton, Victoria, Australia. [9]Department of Chemistry and Centre for Plastic Electronics, Imperial College London, London, UK. [10]King Abdullah University of Science and Technology (KAUST), PSE, Thuwal, Saudi Arabia. *e-mail: hs220@cam.ac.uk

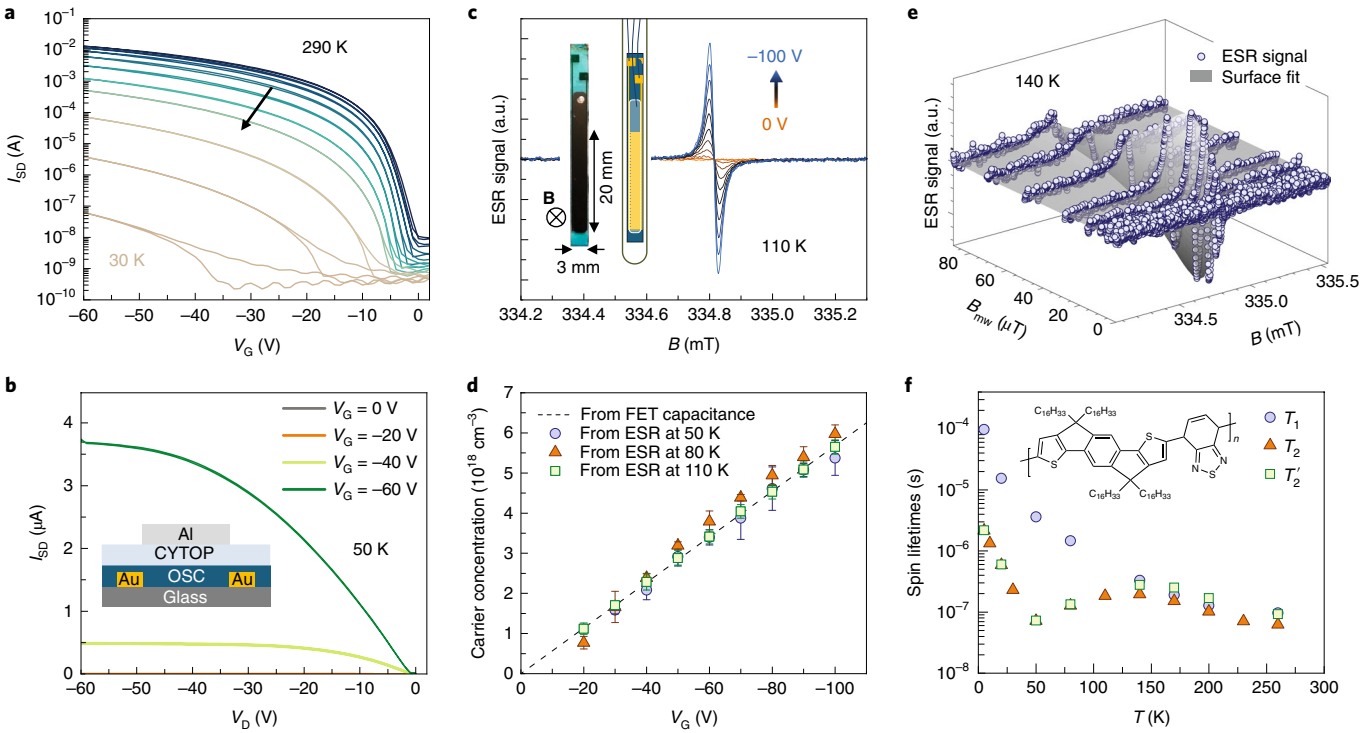

Fig. 1 | IDTBT field-induced ESR devices. a, Source–drain currents I_{SD} in the saturation regime of a representative FET from 290 K to 30 K. **b**, Output curve of the same device at 50 K, showing negligible contact resistance at the onset but a visible threshold voltage shift: I_{SD} vanishes at $V_G = -20$ V. The inset shows a cross-section of the FET architecture with the fluoropolymer CYTOP as a dielectric layer between the organic semiconductor (OSC) and the aluminium gate. **c**, FI-ESR spectra of IDTBT at 110 K for gate voltages of 0 V to −100 V in steps of 10 V. Insets show a photograph and schematic diagram of the device. **d**, Gate-voltage dependence of the spin concentration n_{spin} determined from the Curie magnetic susceptibility at different temperatures and calculated from the FET capacitance (active area of 2.45 × 20 mm^2). Surface concentrations were converted to volumetric concentrations assuming a 2-nm-thick accumulation layer[67]. Error bars represent the standard error from fitting. **e**, ESR spectra of IDTBT at $V_G = -70$ V, 140 K, for increasing microwave (mw) powers, and 2D fit to determine spin lifetimes. **f**, Spin lifetimes T_1, T_2 and T_2' for hole polarons in IDTBT at $V_G = -70$ V.

relaxation times directly and develop a universal model for understanding their spin-relaxation physics. Our selection of polymers includes a semicrystalline, p-type reference system investigated previously by FI-ESR[18], poly(2,5-bis(3-alkylthiophen-2-yl)thieno[3,2-b]thiophene) (pBTTT), together with two high-mobility p-type donor–acceptor copolymers, the nearly amorphous indacenodithiophene-co-benzothiadiazole copolymer (IDTBT)[39] and the highly crystalline diketopyrrolopyrrole-co-benzotriazole (DPP-BTz)[40,41], and one high-mobility n-type copolymer, naphthalenediimide-co-bithiophene, p(NDI2OD-T2)[42]. Chemical structures are given as insets in Figs. 1 and 4. We focus on high-mobility systems not only because we are interested in how spin dynamics is coupled to charge motion, but also because such systems are promising candidates for achieving long spin-diffusion lengths[6,7].

With high hole mobilities of 1–2 cm^2 V^{-1} s^{-1} and exceptionally low energetic disorder despite its nearly amorphous morphology[39] (close inter-chain packing occurs only at isolated contact points), IDTBT is an ideal material in which to investigate spin dynamics. The FI-ESR measurements were performed on IDTBT field-effect transistors (FETs) which show temperature-activated charge transport with ideal FET characteristics down to ~170 K while still remaining operational down to 30 K (Fig. 1; Supplementary Sections 1 and 2). Below 170 K, residual energetic disorder manifests itself in an increase of the threshold voltage and a gate-voltage dependence of the saturation mobility μ_{sat}. We verified that the paramagnetic susceptibility from the ESR spectra matches the gate-induced carrier concentration determined from the dielectric capacitance (Fig. 1c,d; Supplementary Section 3), confirming that we detect all electronically injected spins. The spin-lattice relaxation and coherence times, T_1 and T_2 respectively, can be extracted from the power saturation behaviour and linewidth in continuous-wave ESR[16,19]. We use a similar approach to established literature, but perform a two-dimensional fit to the ESR spectra as a function of magnetic field and microwave power (Fig. 1e; Supplementary Sections 4 and 5). This minimizes errors, especially in T_1, that may otherwise result from fitting noisy spectra individually.

All spectra above 50 K follow the saturation behaviour of a single Lorentzian resonance, showing that spins experience a homogeneous magnetic environment with uniform lifetimes. Below 50 K, spins experience an inhomogeneous environment with varying local HFI and g-tensor fields, resulting in the resonance line becoming a convolution of a Gaussian field distribution with width δB_{rms} and the ever-present Lorentzian broadening of individual spin packets. By fitting the saturation behaviour to the resulting Voigtian lineshape, we determine both δB_{rms} and the intrinsic lifetimes $T_{1,2}$ in this regime.

The extracted spin lifetimes are summarized in Fig. 1f together with $T_2' = (1/T_2 - 1/(2T_1))^{-1}$, which eliminates contributions of spin-lattice relaxation to decoherence[43]. T_1 decreases monotonously with increasing temperature, but from the behaviour of T_2,we can identify three distinct regimes of spin dynamics. (1) Below 50 K, T_2 is smaller than T_1 and decreases gradually with increasing temperature to reach a minimum of 70 ns while the lineshape remains distinctly inhomogeneous. (2) From 50 K to 140 K, the resonance shape becomes Lorentzian with an increasing coherence time of up to 200 ns at 140 K while T_1 continues to decrease. (3) Above 140 K, we reach a high-temperature regime where $T_1 \simeq T_2$ and both lifetimes decrease gradually.

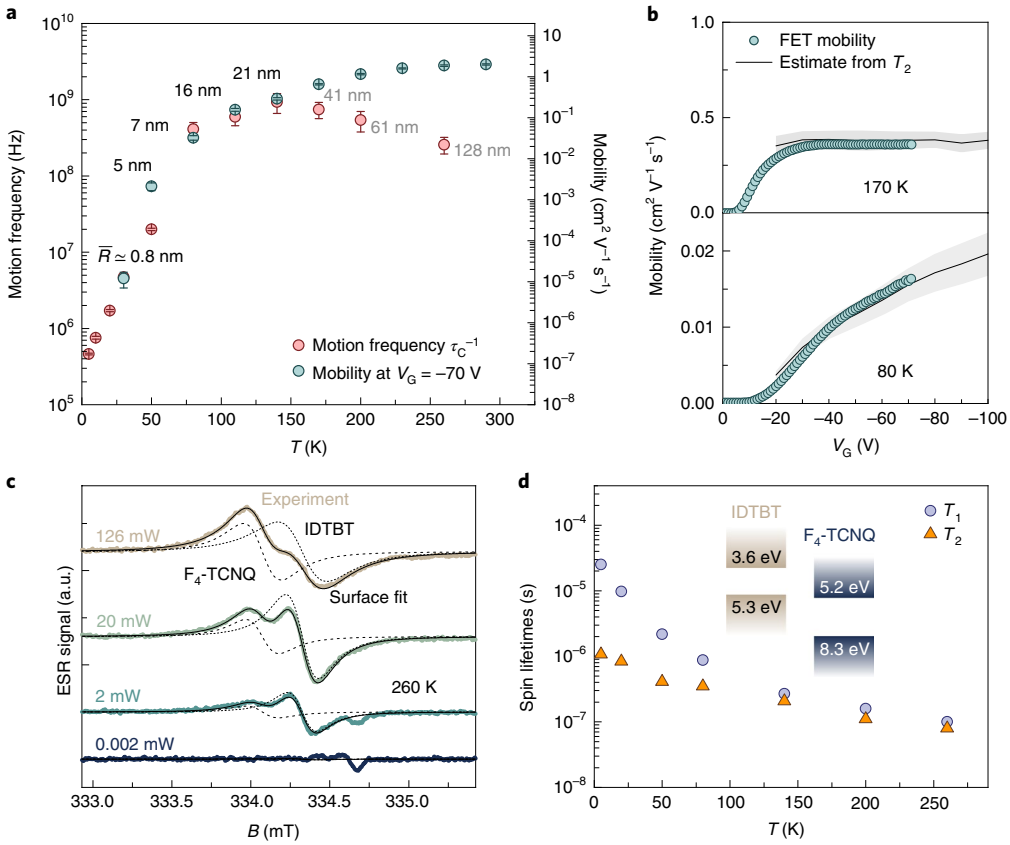

Fig. 2 | Relaxation processes in IDTBT. a, Motion frequency of charges ν determined from T_2' under the assumption of motional relaxation (left axis) and saturation mobilities from FET measurements at $V_G = -70$ V (right axis). Error bars represent the standard error determined by error propagation from the fitting errors of $T_{1,2}$ and δB_{rms}. Labels show the extracted hopping distances $\bar{R}$ by relating the two quantities with the Einstein relation for charge transport. Values above 140 K (light grey) are obtained by extending the motional narrowing model to regime (3) where EY-like relaxation becomes dominant and therefore do not represent actual hopping distances. We do not report a value for $\bar{R}$ at 30 K because the late onset and large leakage current in transfer characteristics at this temperature make it difficult to extract a reliable mobility. **b**, V_G dependence of the FET mobility and predicted mobilities from T_2' at 80 K and 170 K by using the Einstein relation with a fixed $\bar{R}$ from **a**. **c**, Slices from an ESR power saturation scan of doped IDTBT in a polystyrene matrix (260 K). The surface fit of two resonances (solid black lines) is shown together with separate contributions from F_4-TCNQ and IDTBT at $g = 2.00395$ and $g = 2.00243$, respectively (dashed lines). The small signal at 334.7 mT, visible at low microwave powers, comes from a known paramagnetic impurity in the quartz substrate. **d**, Temperature-dependent spin lifetimes of the IDTBT resonance. Inset shows highest occupied and lowest unoccupied molecular orbital (HOMO and LUMO) levels of IDTBT and F_4-TCNQ.

Of the above three regimes, the intermediate one has previously been observed and attributed to 'motional narrowing'[15]. Its physics is elegantly captured by the semi-classical Redfield theory, which understands spin dynamics in terms of stochastic fluctuations of (effective) magnetic fields $B_{eff}(t)$ with amplitudes δB_{rms} and a characteristic frequency τ_c^{-1} (refs. [43,44]). For sufficiently fast fluctuations $\gamma_e \delta B_{rms} \tau_c \ll 1$, the lifetimes are given by[45]

$$T_1^{-1} = \gamma_e^2 \left((\delta B_{rms}^x)^2 + (\delta B_{rms}^y)^2 \right) \frac{\tau_c}{1 + \omega_L^2 \tau_c^2} \quad (1)$$

$$T_2^{-1} = \frac{1}{2T_1} + \gamma_e^2 (\delta B_{rms}^z)^2 \tau_c \quad (2)$$

where the z-axis is defined by the external magnetic field B_0, $\omega_L = \gamma_e B_0$ denotes the Larmor frequency, and γ_e is the electron gyromagnetic ratio. Equations (1) and (2) imply that faster fluctuations result in longer coherence times (motional narrowing) while spin-lattice relaxation is most effective 'on resonance' when $\tau_c^{-1} = \omega_L$. Importantly, equation (2) can be used to determine τ_c if $T_{1,2}$ and δB_{rms} are known.

The transition from an inhomogeneous broadening to a single Lorentzian lineshape at 50 K indicates that the randomly distributed local fields begin to act as fluctuating fields with $\gamma_e \delta B_{rms} \tau_c \ll 1$ due to increasingly rapid charge motion. Local fields no longer appear as static and drive spin relaxation instead of causing a distribution of Zeeman splittings (and resonance position). This is consistent with the decrease of T_1 and increase of T_2 with temperature above 50 K, as predicted from the Redfield equations for $\tau_c^{-1} < \omega_L$. The temperature dependence cannot be explained by smaller local fields δB_{rms}, for instance due to a reduction of HFIs for more delocalized charges[11,46], as this would increase both T_1 and T_2 concurrently. We therefore identify τ_c^{-1} in regime (2) as the hopping frequency ν for charge motion between sites and determine $\delta B_{rms}^z \simeq 0.34$ mT from the Gaussian contribution to the linewidth at 5 K where such motion freezes out. Incidentally, the onset of motional narrowing at 50 K almost coincides with the onset of macroscopic charge transport in FET measurements.

The transition from decreasing to increasing coherence times at the onset of motional narrowing has been theoretically predicted[21,47] but to our knowledge not yet experimentally observed. For $\gamma_e \delta B_{rms} \tau_c > 1$, decoherence takes place only when a spin moves to a different field environment within $\nu^{-1} = \tau_c$ plus the average time

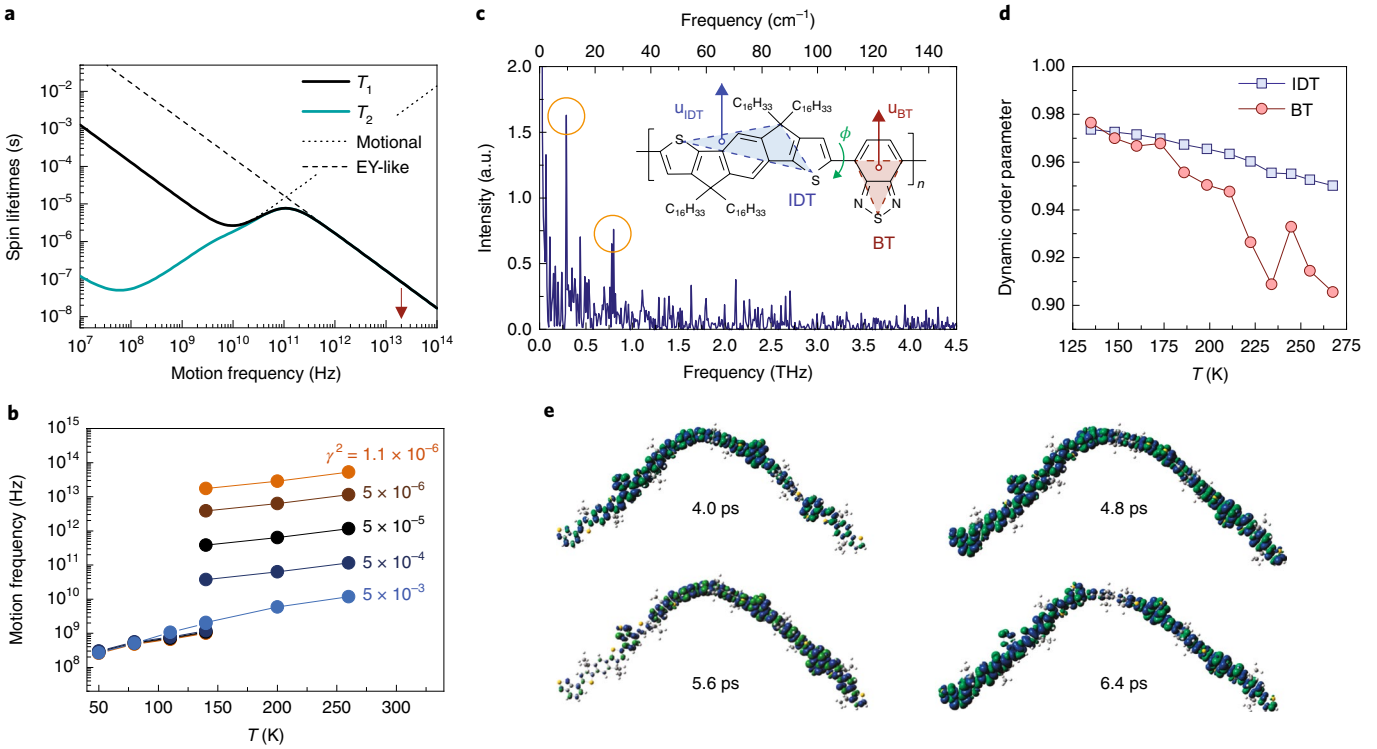

Fig. 3 | Modelling of IDTBT spin dynamics. a, Expected spin lifetimes as a function of motion frequency ν for an experimental value of $\delta B_{rms} = 0.34$ mT and a spin admixture of $\gamma^2 = 1.1 \times 10^{-6}$ from DFT. Dashed and dotted lines extrapolate motional relaxation to higher temperatures and EY-like relaxation to lower temperatures, respectively. The red arrow indicates the required motion frequency to reach the measured coherence time at 260 K. **b**, Required motion frequencies for equation (4) to reach the experimental coherence times in IDTBT. Plots for different values of γ^2 show that a smooth transition between the two regimes of dominant EY-like and motional relaxation can only be achieved for $\gamma^2 \simeq 5 \times 10^{-3}$. **c**, Fourier transform of the torsion angle autocorrelation function for an IDTBT segment of five repeat units, taken from an amorphous morphology. It shows the typical frequencies responsible for the fluctuations in torsion angle with two distinct peaks at 3.0×10^{11} Hz and 6.7×10^{11} Hz (orange circles). Inset shows the chemical structure of an IDTBT repeat unit. Vectors $\mathbf{u}_{IDT}$ and $\mathbf{u}_{BT}$ define orientations of respective conjugated fragments, which are used to calculate the order parameter S. The dihedral angle ϕ, connecting IDT and benzothiadiazole (BT) units, is shown in green. **d**, Dynamic order parameter of IDT and BT fragments as a function of temperature. Note that the temperature has been rescaled to effectively account for quantum effects, which become noticeable at low temperatures (Supplementary Section 13). **e**, Plots of the spin density from DFT (CAM-B3LYP/6-31G** basis set) along an IDTBT chain of five monomers, extracted from the amorphous phase. Representative snapshots are at intervals of 0.8 ps, from a total simulated time evolution of 80 ps.

to lose its initial phase: $T_2' = \tau_c + t_d$, $t_d = (\gamma_e \delta B_{rms})^{-1}$. The transition to a Redfield regime is modelled by attenuating $t_d \rightarrow t_d(1 + t_d/\tau_c)$ according to the reduced dwell time at each site, and the coherence time becomes[47]

$$T_2' = \tau_c + \frac{1}{\gamma_e \delta B_{rms}} + \frac{1}{\gamma_e^2 \delta B_{rms}^2 \tau_c} \quad (3)$$

Equation (3) interpolates between regimes (1) and (2) and enables us to probe charge motion all the way down to 5 K. In Fig. 2a, the motion frequency ν is plotted together with μ_{sat} from FET measurements, both determined at $V_G = -70$ V. ν increases by four orders of magnitude from 0.5 MHz at 5 K (where charge motion is effectively frozen out), to 5 MHz at 30 K (where we start detecting a macroscopic FET current), to 1 GHz at 140 K.

For diffusive charge transport, the hopping rate and mobility are coupled via the Einstein relation $\mu = e\overline{R}^2/(k_B T)\nu$, where e is the elementary charge and $\overline{R}$ denotes the mean hopping distance (see Supplementary Section 6 for a discussion). Estimates for this characteristic length scale (Fig. 2a) range from 5 nm at 50 K, corresponding to three IDTBT repeat units[48], to ~20 nm at 140 K. Moreover, Fig. 2b shows that, for a fixed temperature, the gate voltage (V_G) dependence of μ_{sat} follows the mobilities estimated from T_2' via equation (3) and Einstein's relation, using a constant value of $\overline{R}$ for all gate voltages. This is microscopic evidence for the increase in mobility originating from both faster and longer-range charge motion. The increase of $\overline{R}$ with temperature is expected as more delocalized states at higher energies become occupied[49], and the exceptionally long length scale of ~13 repeat units at 140 K lies within theoretically predicted values of the order of 10 repeat units for hopping along a model polymer chain with low energetic disorder[50]. The minimal amount of backbone torsion[39] and the expected large persistence length in IDTBT[51] corroborate that charge motion does indeed take place over such length scales.

We now turn to discussing spin dynamics in the high-temperature regime (3). Extending the previously established motional relaxation model above 140 K fails for multiple reasons. First, the decrease of T_2 would require us to assume that, by some mechanism, hopping rates decrease with increasing temperature in this regime. However, if there were such a mechanism, it should be reflected by an increase of T_1 with increasing temperature, contrary to observations. Second, the decrease of T_2 stands in contrast to the continuously temperature-activated mobility, leading to extracted motion distances of up to 130 nm at room temperature. Such length scales, of the order of the total polymer chain length, are exceedingly unlikely. We conclude that, in this regime, spin lifetimes must be dominated by an alternative relaxation pathway.

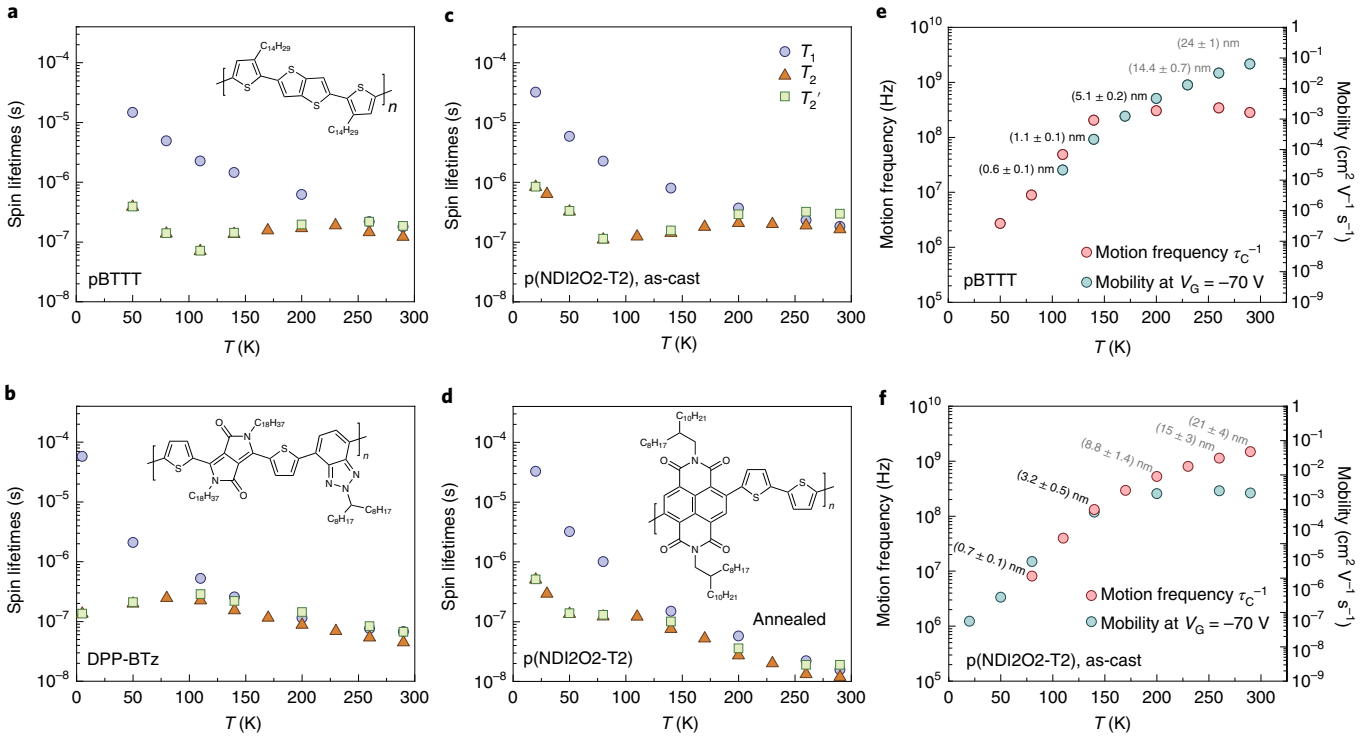

Fig. 4 | Spin lifetimes of field-induced charges. a–d, Lifetimes in pBTTT (**a**), DPP-BTz (**b**) and as-cast and annealed p(NDI2OD-T2) (**c**,**d**), determined by power saturation measurements at gate voltages of −70 V for p-type and 70 V for n-type materials. The low-temperature minima of T_2 coincide with transitions from Voigtians to Lorentzians, except for DPP-BTz that shows a Lorentzian resonance down to 5 K. Insets show schematics of the respective molecular geometries. **e**,**f**, Charge-carrier mobilities from FET characteristics, motion frequencies determined from T_2' (assuming motional relaxation) and resulting distances $\bar{R}$ for pBTTT and as-cast p(NDI2OD-T2) from the Einstein relation for charge transport. Values in light grey are obtained by extending the motional narrowing model to regime (3) where EY-like relaxation becomes dominant and therefore do not represent actual hopping distances. Confidence intervals represent the standard error, determined by error propagation from the fitting errors of $T_{1,2}$ and δB_{rms}.

A potential mechanism was recently discussed by Tsurumi et al.[19], who observed a similar turnaround in the temperature dependence of T_2 above 100 K in single crystals of the small molecule, 3,11-didecyldinaphtho[2,3-d:2′,3′-d′]benzo[1,2-b:4,5-b′]dithiophene (C_{10}-DNBDT). They correlate the spin lifetimes with momentum scattering rates estimated from independent Hall effect measurements and a decreasing mobility at higher temperatures, concluding that conventional EY spin relaxation of charges in a band structure provides the main relaxation pathway. Such an EY explanation due to momentum scattering is clearly not applicable to our system: the hole mobility in IDTBT remains temperature-activated up to 300 K, and there are no signs of coherent charge transport; for example, no Hall effect signature has ever been observed in IDTBT (Supplementary Section 7).

However, a mechanism similar to EY relaxation has been recently proposed for systems with incoherent charge transport in which spatial scattering (that is, hopping) replaces momentum scattering[22,23]. Spin–orbit coupling mixes spin states from different orbitals, as quantified by the dimensionless spin admixture $\gamma^2 \sim \xi^2/(2\Delta)^2$ (where ξ is atomic spin–orbit coupling and Δ is energy difference between mixed orbitals), and transfer integrals become spin-dependent. Such an admixture of spin states enables spin-flips during a hopping event, and the resulting relaxation rates are expected to scale linearly with the hopping frequency: $T_1^{-1} = T_2^{-1} = (3/8)\gamma^2\nu$. Unlike the conventional EY mechanism due to momentum scattering invoked in ref. [19], such a relaxation pathway due to spatial scattering/hopping (referred to as EY-like below) becomes more effective at higher mobilities,as hopping enhances charge transport whereas momentum scattering hinders it. Such a mechanism could qualitatively reproduce the temperature dependence of spin lifetimes in IDTBT.

The total spin relaxation rates are then given by

$$\frac{1}{T_{1,2}} = \frac{1}{T_{1,2}^{M}} + \frac{1}{T_{1,2}^{EY}} \tag{4}$$

where $T_{1,2}^{M}$ and $T_{1,2}^{EY}$ denote the contributions from motional narrowing and EY-like relaxation, respectively. They are plotted in Fig. 3a as a function of motion frequency ν, showing a crossover from motional narrowing to EY-like processes with $T_1 = T_2$ as ν increases. The experimental lifetimes indicate that EY-like relaxation should set in around 140 K. We can determine the required motion frequencies throughout this transition from the experimental coherence times with equation (4). There are always two possible values of ν, to the right and left of the crossover point, both giving the same coherence time (Fig. 3a). Unique values can still be determined with the condition of increasing ν with higher temperatures, and the results are shown in Fig. 3b for different values of γ^2. A smooth increase in motion frequency from the motional narrowing regime below 140 K to the EY-like regime can only be achieved for a high spin admixture of $\gamma^2 \simeq 5 \times 10^{-3}$. For smaller γ^2, reproduction of the experimental values of $T_{1,2}$ requires a sudden jump in motion frequency from 10^9 Hz (which characterizes the motional narrowing regime) to significantly higher values.

We calculated γ^2 from density functional theory (DFT) for a disordered IDTBT morphology (Supplementary Section 8). γ^2 depends

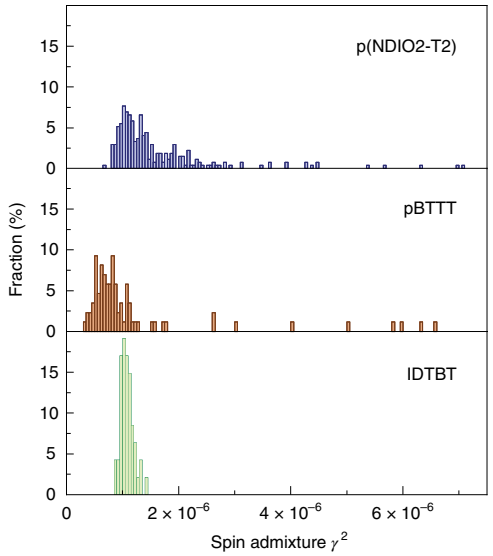

Fig. 5 | Spin admixtures. γ^2 calculated for an amorphous IDTBT morphology and crystalline morphologies of pBTTT and p(NDI2OD-T2). The histograms contain a total of 120, 90 and 275 segments for IDTBT, pBTTT and p(NDI2OD-T2), respectively, and outliers can be traced back to sites with larger backbone torsion. Details of the DFT calculations are given in Supplementary Section 8.

on the relative orientation of neighbouring orbitals and therefore the torsion angles along the polymer backbone[23]. IDTBT exhibits a highly planar backbone, and the resulting histogram of spin admixtures (Fig. 5) shows a narrow distribution around an average of $\gamma^2 = 1.1 \times 10^{-6}$. These values are roughly consistent with the small g-shift of 110 ppm ($g = 2.00243$) in IDTBT. For such small γ^2, motion frequencies of 10–20 THz are needed to reproduce experimental spin lifetimes in the EY-like regime at 260 K. These are of the order of the typical vibrational relaxation time, $\lesssim$1 ps in organic semiconductors, meaning that a treatment of charge dynamics in terms of incoherent hopping breaks down[50]. What could be the origin of such high motion frequencies?

To understand whether the associated charge dynamics involves inter-chain or intra-chain processes, we isolated highly dilute IDTBT chains (0.33 wt%) in an inert polystyrene matrix of comparable molecular weight. A small number of charge carriers were introduced by p-type doping with the small molecule 2,3,5,6-tetrafluoro-7,7,8,8-tetracyanoquinodimethane (F_4-TCNQ) (see Methods). The corresponding ESR spectra at 260 K (Fig. 2c) are successfully fitted over the full range of microwave powers by two distinct resonances at $g = 2.0034$ and $g = 2.00243$. The lower-field resonance can be attributed to F_4-$TCNQ^-$, which has a reported g-factor of ~2.003[52,53], while the higher-field resonance matches exactly with the g-factor of IDTBT found in FI-ESR. Despite being somewhat longer, the extracted spin lifetimes (Fig. 2d) are to those determined from FI-ESR above 140 K, demonstrating that in IDTBT intra-chain relaxation is dominant in this regime.

A potential candidate for such fast intra-chain processes is the vibrational dynamics of the polymer backbone which are sufficiently slow for the charge/spin density distribution to adapt. Those conformational changes cause displacements of the spin density along the backbone that take place on the same timescales as the vibrations themselves and may become fast enough to drive EY-like relaxation. Such an adiabatic shuttling motion of the spin density has so far been neglected in established relaxation theories. To model this, we take snapshots from the temporal evolution of an IDTBT chain segment from molecular dynamics simulations, including both torsional and higher-frequency modes, and determine the spin density distribution of an unpaired charge in intervals of 0.8 ps. We limit our model to a truncated chain segment of five monomers and neglect any inter-chain effects beyond taking the backbone conformations from a full morphology. Figure 3e shows how the resulting spin density contours evolve as a function of time. We can clearly observe displacements of the spin density together with changes to the localization length between the time steps. These adiabatic fluctuations take place at frequencies of 1–10 THz, fast enough to drive the observed spin relaxation even for a small spin admixture of $\gamma^2 = 1.1 \times 10^{-6}$. The associated length scale is comparable to the charge coherence length and smaller than the mean free path of charge carriers. The charge carrier mobility therefore remains limited by the incoherent hopping processes over longer length scales, between sites that are defined by the static energetic disorder in the network of polymer chains—as analysed above in the motional narrowing regime.

To understand the temperature dependence of the vibrational dynamics, we performed molecular dynamics simulations and extracted the dominant frequencies from the torsional angle autocorrelation function of an IDTBT chain within a simulated morphology (Fig. 3c). The lowest torsional modes are predicted at 0.2 THz for an isolated IDTBT monomer and around 0.3 THz for a chain segment from a disordered morphology. Higher-energy modes will provide additional relaxation pathways, although it is expected that higher frequencies and smaller amplitudes will be less effective at coupling to the spin (equations (1) and (2)). We also modelled the temperature dependence of the torsional dynamics and evaluated the dynamic order parameter S for torsional fluctuations of the IDT and BT conjugated units[54,55] between 100 K and 300 K (see Methods for computational details). Calculated order parameters (Fig. 3d) decrease with higher temperatures, owing to the thermal activation of modes. Interestingly, around 170 K, close to the temperature at which we observe the crossover to the high-temperature spin relaxation regime, a torsional motion of the BT units sets in that causes a pronounced reduction of the corresponding order parameter. This is further evidence for the proposed link between spin relaxation and structural dynamics. On the other hand, the mere modulation of HFI- and g-tensors with torsional modes, while the charge density remains statically localized at a site, is insufficient to reproduce the observed spin lifetimes (Supplementary Section 9).

We conclude that spin relaxation in IDTBT at high temperatures can be consistently explained by rapid, intra-chain shuttling of the spin density as it adapts to vibrational modes. Low-frequency modes effect larger atomic displacements and should therefore impact the spin density more strongly, but higher-frequency modes may also contribute. Anderson et al. recently showed that carbon–carbon stretching modes around 1,000 cm^{-1} (30 THz) can drive considerable displacements of the charge density, causing pronounced absorption features in the near-infrared range[56]. As the temperature increases beyond 140 K, such modes will gradually become populated, further enhancing spin-density fluctuations and relaxation.

Armed with this understanding, we now turn to investigating spin relaxation in more complicated, semicrystalline systems, in which inter-chain processes are also likely to contribute. pBTTT and p(NDI2OD-T2) are widely studied p-type and n-type conjugated polymers, respectively, with field-effect mobilities of 0.1–0.5 $cm^2 V^{-1} s^{-1}$ (refs. [42,57]), while DPP-BTz, with a hole mobility of 1–2 $cm^2 V^{-1} s^{-1}$ belongs to an emerging class of high-performance ambipolar copolymers[40]. p(NDI2OD-T2) is a particularly interesting system because it is possible to tune the size of the crystalline domains by processing while keeping other properties, such as cumulative positional disorder and energetic disorder in the crystalline domains, largely unaffected[58,59].

Figure 4 gives an overview of measured spin lifetimes. All four materials exhibit clear motional narrowing and EY-like, high-temperature

relaxation regimes similar to IDTBT, which demonstrates the generality of our observations. However, there are clear differences in onset of the different regimes and in magnitude of the spin relaxation times. The onset of motional narrowing, observed at 50 K for IDTBT, shifts up to 80 K and 110 K for as-cast p(NDI2OD-T2) and pBTTT, respectively, indicating suppressed charge motion at the lowest temperatures. DPP-BTz stands out by exhibiting Lorentzian lineshapes down to 5 K, showing that charge motion remains sufficiently fast to average over HFI and g-tensor fields. We are therefore unable to estimate δB_{rms} and determine motion frequencies for DPP-BTz. However, from comparison to other polymers, ν is likely to exceed 10^7 Hz even at 5 K, consistent with the exceptionally high charge-carrier mobilities measured in this system[41]. Motion frequencies and distances for pBTTT and as-cast p(NDI2OD-T2) are given in Fig. 4e,f and reach values of 0.2–0.3 GHz around 200 K. Comparing charge dynamics at 140 K to IDTBT, we see that the lower mobilities of pBTTT and p(NDI2OD-T2) are reflected by five-to-ten-times slower charge motion ($\nu \simeq 0.1$–0.2 GHz) and significantly shorter length scales of 1–3 nm. This is consistent with previous reports of exceptionally low energetic disorder in IDTBT[39]. All polymers also exhibit a similar high-temperature regime with decreasing lifetimes $T_1 \simeq T_2$. The onset takes place at similar temperatures of 230 K and 200 K for pBTTT and as-cast p(NDI2OD-T2), respectively, but shifts down to 110 K for annealed p(NDI2OD-T2) and DPP-BTz films. In fact, room-temperature coherence times in p(NDI2OD-T2) are reduced by an order of magnitude upon annealing. This is striking and shows that spin dynamics for the same polymer can be changed considerably by tuning its morphology.

In polymers such as p(NDI2OD-T2) there is clear evidence that all charge carriers reside within the crystalline domains[58], regardless of the degree of crystallinity. Grazing incidence wide angle X-ray scattering (GIWAXS) measurements probing these domains show that thermal annealing of p(NDI2OD-T2) increases the coherence length of stacking along all three crystallographic directions, with an increase of in-plane (IP) coherence lengths from 16.5 to 20.7 nm along the backbone direction and from 20 to 38 nm along the lamellar stacking direction (Supplementary Section 10). Such an enlargement of crystallites and the ensuing reduced orientational disorder is unlikely to cause larger spin admixtures or more pronounced torsional dynamics (see Supplementary Sections 11 and 12). The apparent relationship between in-plane crystallite size and the onset of the EY-like regime extends beyond p(NDI2OD-T2) to the other two polymer systems. DPP-BTz exhibits IP spacing coherence lengths of 30 nm[41], approaching those of annealed p(NDI2OD-T2), whereas the ribbon phase of pBTTT exhibits much smaller coherence lengths on the scale of ~7 nm (despite showing micrometre-sized topographic features)[60–62]. IDTBT, as a point of reference, is the least crystalline of the above systems, with coherence lengths of 4.9 nm and 3.3 nm for lamellar and π-π spacing, respectively[48].

To explain this pronounced dependence of the spin relaxation time on crystallinity, we propose that for crystalline polymers, in addition to the fast intra-chain charge dynamics, the analogous inter-chain, intra-crystallite dynamics of the charge density coupled to vibrational modes contribute to an EY-like process. Ab-initio calculations and charge accumulation spectroscopy measurements have demonstrated that polarons in crystalline polymers such as pBTTT and p3HT are delocalized over several π-stacked chains[49,63,64]. This implies that in such crystalline polymers the vibrational dynamics of the chains within the crystallites on a picosecond timescale will not only cause the wavefunction to oscillate along the backbone direction, but also along the π-π stacking direction. This is similar to the 'transient localization' of wavefunctions in molecular crystals which involves a similar 'surfing' motion of the electron wavefunction on the waves of molecular lattice distortion[65].

In this regime, the carrier wavefunction explores on a picosecond timescale a relatively extended volume along both the intra- and inter-chain direction, and spin relaxation remains a consequence of the finite spin–orbit coupling spin admixture that is present within this relevant volume. We carried out similar DFT calculations as for IDTBT for crystalline morphologies of pBTTT and p(NDI2OD-T2) to determine the distribution of γ^2 across different sites in the morphologies (Fig. 5). γ^2 is largest for p(NDI2OD-T2), with a distribution in the range of $(1–3)\times10^{-6}$ reflecting the large torsion angle of ~41° between NDI and T units[66]. pBTTT has the smallest γ^2—in the range of $(0.2–1.0)\times10^{-6}$—reflecting the near-planar backbone conformation in the high crystalline polymer domains. This trend appears consistent with the observed spin relaxation times at room temperature being shortest in annealed p(NDI2OD-T2) and longest in pBTTT. However, the quantitative interpretation is likely to be more complicated as both polymers consistently show a number of outliers up to $\gamma^2 \sim 7\times10^{-6}$ compared to the narrow distribution of spin admixtures in IDTBT. Such sites with varying backbone geometry could potentially contribute to the observed spin relaxation times: increasing the size of crystallites by annealing, for example, will allow polarons to sample a larger part of the γ^2 distribution and experience stronger spin-flip relaxation. This could explain the large difference in spin relaxation time between as-cast and annealed p(NDI2OD-T2).

In this work, we have established a general framework for understanding spin-relaxation mechanisms in high-mobility conjugated polymers that also gives microscopic insight into the charge dynamics. At low and intermediate temperatures polaron spin dynamics are driven by charge motion through a static environment of local HFI fields and g-tensor anisotropies. The coherence time undergoes a distinct transition at the onset of motional narrowing, and we can quantify the charge's motion frequency throughout this transition and down to temperatures where electrical measurements are no longer possible. Spin coherence times therefore serve as a quantitative probe for hopping frequencies, which form the basis of charge transport simulations but typically remain elusive to the experimentalist. At higher temperatures, a previously unidentified EY-like process becomes the dominant relaxation pathway. This takes place on significantly faster timescales than the motion that determines the FET mobility and is governed by oscillations of the charge wavefunction on picosecond timescales due to transient localization. These are driven by the structural, vibrational dynamics and cause spin relaxation through spin–orbit coupling and the local distribution of γ^2 values. Although our model provides a consistent explanation of the observations, there is scope for improving the theoretical model in the future, as the simple EY-like relaxation model was originally developed for incoherent hopping is not fully applicable to describing the adiabatic charge dynamics relevant here.

Our work also establishes a clear link between the surprisingly similar spin dynamics of high-mobility conjugated polymers and of molecular crystals[19]. It is unlikely that the more conventional EY momentum scattering that was proposed in ref. [19] is applicable to the polymer systems studied here, but we believe that the results could be explained consistently by assuming that, near room temperature, spin relaxation in both molecular crystals and conjugated polymers is driven by a similar transient localization mechanism. At present, very different models are used for describing charge transport in molecular and polymeric systems, the former being considered more similar to band-like inorganic semiconductors, whereas the latter are considered hopping transport systems. Our study demonstrates a close similarity in their microscopic transport physics. This similarity is masked when measuring electrical transport coefficients, such as the temperature-dependent carrier mobility, which are affected by long-range energetic disorder, but is revealed in our spin relaxation experiments, which provide a more local probe of the charge dynamics.

Understanding of this fascinating transport regime where charge, spin and structural dynamics are so intimately coupled also allows molecular design guidelines to be established for the targeted

development of systems that support both efficient charge transport and long spin lifetimes. By tuning the polymer morphology to achieve low torsional disorder and to stiffen the vibrational modes that cause the rapid oscillations of spin density, we anticipate that microsecond room-temperature spin lifetimes should be achievable in high-mobility polymers. Already, polymers such as pBTTT with spin diffusion lengths of more than 1 μm, despite still comparatively short spin lifetimes[7], are among the best spin conductors reported, and our work lays the foundations for a targeted molecular design effort to achieve even longer spin lifetimes and diffusion lengths.

Online content

Any methods, additional references, Nature Research reporting summaries, source data, statements of code and data availability and associated accession codes are available at https://doi.org/10.1038/s41567-019-0538-0.

Received: 15 December 2018; Accepted: 18 April 2019;
Published online: 3 June 2019

References

1. Di, D. et al. High-performance light-emitting diodes based on carbene–metal-amides. *Science* **356**, 159–163 (2017).
2. Weiss, L. R. et al. Strongly exchange-coupled triplet pairs in an organic semiconductor. *Nat. Phys.* **13**, 176–181 (2017).
3. Rao, A. & Friend, R. H. Harnessing singlet exciton fission to break the Shockley–Queisser limit. *Nat. Rev. Mater.* **2**, 17063–12 (2017).
4. Wagemans, W. & Koopmans, B. Spin transport and magnetoresistance in organic semiconductors. *Phys. Status Solidi B* **248**, 1029–1041 (2011).
5. Wohlgenannt, M. Organic magnetoresistance and spin diffusion in organic semiconductor thin film devices. *Phys. Status Solidi Rapid. Res. Lett.* **6**, 229–242 (2012).
6. Watanabe, S. et al. Polaron spin current transport in organic semiconductors. *Nat. Phys.* **10**, 308–313 (2014).
7. Wang, S.-J. et al. Long spin diffusion lengths in doped conjugated polymers due to enhanced exchange coupling. *Nat. Electron.* **2**, 98–107 (2019).
8. Ando, K., Watanabe, S., Mooser, S., Saitoh, E. & Sirringhaus, H. Solution-processed organic spin–charge converter. *Nat. Mater.* **12**, 622–627 (2013).
9. Sun, D. et al. Inverse spin Hall effect from pulsed spin current in organic semiconductors with tunable spin–orbit coupling. *Nat. Mater.* **15**, 863–869 (2016).
10. Sanvito, S. The rise of spinterface science. *Nat. Phys.* **6**, 562–564 (2010).
11. Shao, M. et al. The isotopic effects of deuteration on optoelectronic properties of conducting polymers. *Nat. Commun.* **5**, 3180 (2014).
12. Steyrleuthner, R. et al. Impact of morphology on polaron delocalization in a semicrystalline conjugated polymer. *Phys. Chem. Chem. Phys.* **19**, 3627–3639 (2017).
13. Schott, S. et al. Tuning the effective spin–orbit coupling in molecular semiconductors. *Nat. Commun.* **8**, 15200 (2017).
14. McNellis, E. R., Schott, S., Sirringhaus, H. & Sinova, J. Molecular tuning of the magnetic response in organic semiconductors. *Phys. Rev. Mater.* **2**, 074405 (2018).
15. Matsui, H., Hasegawa, T., Tokura, Y., Hiraoka, M. & Yamada, T. Polaron motional narrowing of electron spin resonance in organic field-effect transistors. *Phys. Rev. Lett.* **100**, 126601 (2008).
16. Matsui, H., Mishchenko, A. S. & Hasegawa, T. Distribution of localized states from fine analysis of electron spin resonance spectra in organic transistors. *Phys. Rev. Lett.* **104**, 056602 (2010).
17. Marumoto, K. et al. Microscopic mechanisms behind the high mobility in rubrene single-crystal transistors as revealed by field-induced electron spin resonance. *Phys. Rev. B* **83**, 075302 (2011).
18. Matsui, H. et al. Correlation between interdomain carrier hopping and apparent mobility in polycrystalline organic transistors as investigated by electron spin resonance. *Phys. Rev. B* **85**, 035308 (2012).
19. Tsurumi, J. et al. Coexistence of ultra-long spin relaxation time and coherent charge transport in organic single-crystal semiconductors. *Nat. Phys.* **13**, 994–998 (2017).
20. Harmon, N. J. & Flatté, M. E. Distinguishing spin relaxation mechanisms in organic semiconductors. *Phys. Rev. Lett.* **110**, 176602 (2013).
21. Yu, Z. G., Ding, F. & Wang, H. Hyperfine interaction and its effects on spin dynamics in organic solids. *Phys. Rev. B* **87**, 205446 (2013).
22. Yu, Z. G. Spin–orbit coupling, spin relaxation, and spin diffusion in organic solids. *Phys. Rev. Lett.* **106**, 106602 (2011).
23. Yu, Z. G. Spin–orbit coupling and its effects in organic solids. *Phys. Rev. B* **85**, 115201 (2012).
24. Yu, Z. G. Microscopic theory of electron spin relaxation in $N@C_{60}$. *Phys. Rev. B* **77**, 821–826 (2008).
25. Xiong, Z. H., Wu, D., Valy Vardeny, Z. & Shi, J. Giant magnetoresistance in organic spin-valves. *Nature* **427**, 821–824 (2004).
26. Pramanik, S. et al. Observation of extremely long spin relaxation times in an organic nanowire spin valve. *Nat. Nanotechnol.* **2**, 216–219 (2007).
27. Shim, J. H. et al. Large spin diffusion length in an amorphous organic semiconductor. *Phys. Rev. Lett.* **100**, 226603 (2008).
28. Mooser, S., Cooper, J. F. K., Banger, K. K., Wunderlich, J. & Sirringhaus, H. Spin injection and transport in a solution-processed organic semiconductor at room temperature. *Phys. Rev. B* **85**, 235202 (2012).
29. Jiang, S. W. et al. Exchange-dominated pure spin current transport in Alq_3 molecules. *Phys. Rev. Lett.* **115**, 086601 (2015).
30. McCamey, D. R. et al. Hyperfine-field-mediated spin beating in electrostatically bound charge carrier pairs. *Phys. Rev. Lett.* **104**, 13–14 (2010).
31. Nguyen, T. D., Gautam, B. R., Ehrenfreund, E. & Vardeny, Z. V. Magnetoconductance response in unipolar and bipolar organic diodes at ultrasmall fields. *Phys. Rev. Lett.* **105**, 166804 (2010).
32. Szulczewski, G., Sanvito, S. & Coey, M. A spin of their own. *Nat. Mater.* **8**, 693–695 (2009).
33. Grünewald, M. et al. Tunneling anisotropic magnetoresistance in organic spin valves. *Phys. Rev. B* **84**, 125208 (2011).
34. Grünewald, M. et al. Vertical organic spin valves in perpendicular magnetic fields. *Phys. Rev. B* **88**, 085319 (2013).
35. Wid, O. et al. Investigation of the unidirectional spin heat conveyer effect in a 200 nm thin yttrium iron garnet film. *Sci. Rep.* **6**, 28233 (2016).
36. Li, L., Lu, N., Liu, M. & Bässler, H. General Einstein relation model in disordered organic semiconductors under quasiequilibrium. *Phys. Rev. B* **90**, 214107 (2014).
37. Wetzelaer, G. A. H., Koster, L. J. A. & Blom, P. W. M. Validity of the Einstein relation in disordered organic semiconductors. *Phys. Rev. Lett.* **107**, 066605 (2011).
38. Yu, Z. G. Suppression of the Hanle effect in organic spintronic devices. *Phys. Rev. Lett.* **111**, 016601 (2013).
39. Venkateshvaran, D. et al. Approaching disorder-free transport in high-mobility conjugated polymers. *Nature* **515**, 384–388 (2014).
40. Gruber, M. et al. Enabling high-mobility, ambipolar charge-transport in a DPP-benzotriazole copolymer by side-chain engineering. *Chem. Sci.* **6**, 6949–6960 (2015).
41. Schott, S. et al. Charge-transport anisotropy in a uniaxially aligned diketopyrrolopyrrole-based copolymer. *Adv. Mater.* **27**, 7356–7364 (2015).
42. Yan, H. et al. A high-mobility electron-transporting polymer for printed transistors. *Nature* **457**, 679–686 (2009).
43. Abragam, A. *The Principles of Nuclear Magnetism* (Oxford University Press, 1961).
44. Redfield, A. G. On the theory of relaxation processes. *IBM J. Res. Dev.* **1**, 19–31 (1957).
45. Slichter, C. P. *Principles of Magnetic Resonance* (Springer, 2013).
46. Mishchenko, A. S., Matsui, H. & Hasegawa, T. Distribution of localized states from fine analysis of electron spin resonance spectra of organic semiconductors: physical meaning and methodology. *Phys. Rev. B* **85**, 085211 (2012).
47. Baker, W. J., Keevers, T. L., Lupton, J. M., McCamey, D. R. & Boehme, C. Slow hopping and spin dephasing of coulombically bound polaron pairs in an organic semiconductor at room temperature. *Phys. Rev. Lett.* **108**, 267601 (2012).
48. Zhang, X. et al. Molecular origin of high field-effect mobility in an indacenodithiophene–benzo-thiadiazole copolymer. *Nat. Commun.* **4**, 2238 (2013).
49. Liu, T. & Troisi, A. Understanding the microscopic origin of the very high charge mobility in PBTTT: tolerance of thermal disorder. *Adv. Funct. Mater.* **24**, 925–933 (2013).
50. Fornari, R. P. & Troisi, A. Theory of charge hopping along a disordered polymer chain. *Phys. Chem. Chem. Phys.* **16**, 9997–10007 (2014).
51. Vezie, M. S. et al. Exploring the origin of high optical absorption in conjugated polymers. *Nat. Mater.* **15**, 746–753 (2016).
52. Kang, K. et al. 2D coherent charge transport in highly ordered conducting polymers doped by solid state diffusion. *Nat. Mater.* **15**, 896–902 (2016).
53. Fujimoto, R. et al. Molecular doping in organic semiconductors: fully solution-processed, vacuum-free doping with metal–organic complexes in an orthogonal solvent. *J. Mater. Chem. C.* **5**, 12023–12030 (2017).
54. Marcon, V. et al. Understanding structure–mobility relations for perylene tetracarboxydiimide derivatives. *J. Am. Chem. Soc.* **131**, 11426–11432 (2009).
55. May, F., Marcon, V., Hansen, M. R., Grozema, F. & Andrienko, D. Relationship between supramolecular assembly and charge-carrier mobility in perylenediimide derivatives: the impact of side chains. *J. Mater. Chem.* **21**, 9538–9545 (2011).
56. Anderson, M. et al. Displacement of polarons by vibrational modes in doped conjugated polymers. *Phys. Rev. Mater.* **1**, 055604–055609 (2017).

57. McCulloch, I. et al. Liquid-crystalline semiconducting polymers with high charge-carrier mobility. *Nat. Mater.* **5**, 328–333 (2006).
58. Di Pietro, R. et al. Coulomb enhanced charge transport in semicrystalline polymer semiconductors. *Adv. Funct. Mater.* **26**, 8011–8022 (2016).
59. Statz, M. et al. On the manifestation of electron–electron interactions in the thermoelectric response of semicrystalline conjugated polymers with low energetic disorder. *Commun. Phys.* **1**, 1319 (2018).
60. DeLongchamp, D. M. et al. Controlling the orientation of terraced nanoscale 'ribbons' of a poly(thiophene) semiconductor. *ACS Nano* **3**, 780–787 (2009).
61. Wang, C. et al. Microstructural origin of high mobility in high-performance poly(thieno-thiophene) thin-film transistors. *Adv. Mater.* **22**, 697–701 (2010).
62. Schuettfort, T. et al. Microstructure of polycrystalline pBTTT films: domain mapping and structure formation. *ACS Nano* **6**, 1849–1864 (2012).
63. Beljonne, D. et al. Optical signature of delocalized polarons in conjugated polymers. *Adv. Funct. Mater.* **11**, 229–234 (2001).
64. Chew, A. R. et al. Unraveling the effect of conformational and electronic disorder in the charge transport processes of semiconducting polymers. *Adv. Funct. Mater.* **28**, 1804142 (2018).
65. Fratini, S., Mayou, D. & Ciuchi, S. The transient localization scenario for charge transport in crystalline organic materials. *Adv. Funct. Mater.* **26**, 2292–2315 (2016).
66. Lemaur, V. et al. On the supramolecular packing of high electron mobility naphthalene diimide copolymers: the perfect registry of asymmetric branched alkyl side chains. *Macromolecules* **46**, 8171–8178 (2013).
67. Kronemeijer, A. J. et al. Two-dimensional carrier distribution in top-gate polymer field-effect transistors: correlation between width of density of localized states and Urbach energy. *Adv. Mater.* **26**, 728–733 (2014).

Acknowledgements

Funding from ERC Synergy grant SC2 (no. 610115), the Alexander von Humboldt Foundation and the Transregional Collaborative Research Center (SFB/TRR) 173 SPIN+X is acknowledged. S.S. thanks the Winton Programme for the Physics of Sustainability and the Engineering and Physical Sciences Research Council (EPSRC) for funding as well as Z.-G. Yu for discussions, R. Chakalov for assistance with sample fabrication and S.-i. Kuroda, H. Tanaka and S. Watanabe for training and discussions. U.C. is a recipient of a DFG-funded position through the Excellence Initiative by the Graduate School Materials Science in Mainz (GSC 266). The work in Mons was supported by the European Commission/Région Wallonne (FEDER–BIORGEL project), the Consortium des Équipements de Calcul Intensif (CÉCI), funded by the Fonds National de la Recherche Scientifique (FRS-FNRS) under grant no. 2.5020.11 as well as the Tier-1 supercomputer of the Fédération Wallonie-Bruxelles, infrastructure funded by the Walloon Region under grant agreement n1117545, and FRS-FNRS. D.B. is FNRS Research Director. This research was undertaken in part on the SAXS/WAXS beamline at the Australian Synchrotron, part of ANSTO.

Author contributions

S.S. fabricated the FI-ESR devices and carried out the ESR experiments and analyses. R.L.C. performed the Raman measurements. R.D.P. developed the methods to tune the crystallinity of p(NDI2O–T2) and helped with both the fabrication of samples and the interpretation of results. X.J. and C.R.M. carried out the GIWAXS measurements and analysed the GIWAXS data. I.R. carried out and analysed the Hall effect measurements. U.C. and E.R.M. performed the calculation and analyses of spin admixtures. A.Melnyk and D.A. carried out the simulations of dynamic disorder in IDTBT. Y.O., V.L. and D.B. performed the calculations of torsional autocorrelation functions and intra-chain spin density dynamics. C.J., M.L., A.Marks and I.M. synthesized the materials. S.S. and H.S. wrote the manuscript with input from all authors. H.S. and J.S. supervised the project. All authors discussed the results.

Competing interests

The authors declare no competing interests.

Additional information

Supplementary information is available for this paper at https://doi.org/10.1038/s41567-019-0538-0.

Reprints and permissions information is available at www.nature.com/reprints.

Correspondence and requests for materials should be addressed to H.S.

Journal peer review information: *Nature Physics* thanks Z. Valy Vardeny, Zhi-Gang Yu and the other, anonymous, reviewer(s) for their contribution to the peer review of this work.

Methods

Device fabrication. FI-ESR studies are experimentally challenging. They require fabrication of an FET on a narrow yet elongated substrate to fit inside the ESR cavity. The devices also must be electrically stable during the week-long acquisition time required for a full set of temperature, gate-voltage and microwave-power-dependent measurements.

We fabricated top-gate, bottom-contact FETs by spin-coating the polymer and dielectric layers on $40\times40\,mm^2$ quartz substrates and subsequently separating them into individual $3\times40\,mm^2$ devices. Interdigitated source and drain electrodes, with a channel length of 100 µm and an overall width of 24.3 mm, were photolithographically patterned on the quartz substrate. Each device has an active area of $2.45\times20\,mm^2$, and evaporated gold pads allow electrical contact outside the ESR cavity (schematic and photograph shown in Fig. 1c). We used the fluoropolymer CYTOP (Asahi Glass) as a gate dielectric for pBTTT and IDTBT, and poly(methyl methacrylate) for DPP-BTz and p(NDI2OD-T2). A 30-nm-thick aluminium gate electrode was deposited on all devices by shadow-mask evaporation.

Following the work of Nikolka et al.[68], IDTBT films were spin-coated from a $10\,mg\,ml^{-1}$ solution of polymer in equal parts of 1,2-dichlorobenzene (DCB) and chloroform with 7.5 wt% of the small molecule tetracyanoquinodimethane (TCNQ) and annealed at 80 °C for 60 min. The additive TCNQ was shown to passivate the effect of residual water in the polymer film, which may otherwise act as polaron traps and degrade the device performance. TCNQ, however, does not dope IDTBT[68], as was confirmed by full disappearance of the polaron ESR signal at zero gate voltage (see Fig. 1c). Any bulk doping would produce a signal from the full thickness of the film and should therefore be amplified compared to a signal from field-induced charges residing in the accumulation layer only.

pBTTT was spin-coated at 1,500 r.p.m from a $10\,mg\,ml^{-1}$ solution in DCB, DPP-BTz was spin-coated from a $10\,mg\,ml^{-1}$ solution in chlorobenzene, and p(NDI2OD-T2) was spin-coated at 2,000 r.p.m. from a $5\,mg\,ml^{-1}$ solution in toluene. pBTTT and DPP-BTz films were respectively annealed at 180 °C and 110 °C after spin-coating. p(NDI2OD-T2) films were selectively dried in vacuum ('as-cast') or annealed at 200 °C ('annealed'), resulting in an estimated increase of the crystallite volume by a factor of 4, together with a more pronounced face-on orientation (Supplementary Section 10).

We provide further information on the fabrication process in Supplementary Section 1.

ESR measurements. All ESR measurements in this work were carried out on a Bruker E500 spectrometer with an X-band microwave source and Bruker's ER 4122SHQE cavity. Low-temperature measurements were performed with an Oxford Instruments ESR900 helium cryostat, controlled through a MercuryiTC temperature controller. Electrical measurements and biasing of devices mounted in the ESR set-up were performed with a Keithley 2602b with dual source measurement units. All measurements were controlled by CustomXepr, a self-developed Python software enabling the integrated control of all three instruments and the scheduling of automated measurements and temperature cycles.

Polystyrene:IDTBT films. The films were spin-coated at 1200 rpm from a $30\,mg\,ml^{-1}$ solution of polystyrene in DCB with an added 0.33 wt% of IDTBT. Similar to the FI-ESR sample processing, films were deposited on $40\times40\,mm^2$ pre-grooved glass-slides and then separated into $3\times40\,mm^2$ large samples. Charge carriers were introduced by thermally evaporating 100 nm of F_4-TCNQ on top of the films.

We confirmed that these samples were not conductive, consistent with similar results on pBTTT (where charge transport breaks down at concentrations below 2 wt%[69]). Moreover, owed to the weak interactions between polymer chains, IDTBT is unlikely to aggregate either in the polystyrene solution or the resulting thin film. Furthermore, each of the resonances corresponds to $(1.9\pm0.1)\times10^{11}$ spins at 290 K, confirming equal numbers of dopant ions and polarons. The resulting carrier concentration of $\sim5\times10^{17}\,cm^{-3}$ at 290 K (per volume of IDTBT, assuming similar weight-to-volume ratios for IDTBT and polystyrene) is lower than in FI-ESR devices. Both dopant and polaron spin concentrations are temperature-activated, which may reflect the weak energetic driving force for electron transfer to F_4-TCNQ (see inset in Fig. 2d, ref.[68]).

At low temperatures, the IDTBT:polystyrene samples show consistently longer coherence times than the IDTBT FI-ESR devices, together with a larger Gaussian contribution to the lineshape. No clear motional narrowing regime is observed. Such a suppression for isolated IDTBT chains could be attributed to a more localized nature of the polaron states in IDTBT created by doping with F_4-TCNQ, but it may also indicate that motional narrowing in neat IDTBT occurs mainly by incoherent inter-chain hopping between IDTBT chain segments at points where neighbouring chains come close. In either case, these results establish that spin relaxation in IDTBT at high temperatures must be dominated by a thermally activated intra-chain process with characteristic frequencies exceeding the Larmor frequency.

Dynamic order parameter. To simulate torsional dynamics in IDTBT, we first constructed a unit cell and built a supercell of 8 lamellae × 16 chains, that is, 128 tetramers in total. The supercell was equilibrated for 1 ns in the isothermal–isobaric (NTP) ensemble at 100 K. Morphologies were then simulated in the temperature range 100 K to 300 K, at a 10 K step. These trajectories, 1,000 snapshots each, were used for further analysis. Computational details are given in Supplementary Section 13.

The dynamic order parameter S, calculated individually for IDT and BT units, is determined by the normal vectors $\mathbf{u}^{(i)}$ of the conjugated planes, shown in Fig. 3c:

$$S=\left\langle \frac{1}{N}\sum_{i=1}^{N}\left[\frac{3}{2}\left(\mathbf{U}^{(i)}\cdot\mathbf{u}^{(i)}\right)^2-\frac{1}{2}\right]\right\rangle \tag{5}$$

Here, the sum runs over N equivalent fragments, $\langle\ldots\rangle$ indicates time averaging, and $\mathbf{U}^{(i)}=\langle\mathbf{u}^{(i)}\rangle$ is the time-averaged normal verctor. The order parameter is close to one if a fragment retains its orientation through time and vanishes for a uniformly rotating fragment.

Calculated order parameters are shown in Fig. 3d. Note that the temperature dependence is rescaled to effectively account for quantum effects, which become noticeable at low temperatures (Supplementary Note 13).

Data availability

The data underlying this publication are available on the University of Cambridge data repository at https://doi.org/10.17863/CAM.34786.

Code availability

The CustomXepr source code is published at https://github.com/OE-FET/CustomXepr.

References

68. Nikolka, M. et al. High operational and environmental stability of high-mobility conjugated polymer field-effect transistors through the use of molecular additives. *Nat. Mater.* **16**, 356–362 (2016).
69. Lu, G. et al. Moderate doping leads to high performance of semiconductor/insulator polymer blend transistors. *Nat. Commun.* **4**, 1588 (2013).